Vibration Energy Harvesting for Aircraft, Trains and Boats

Genevieve A. Hart (1), Scott D. Moss (1), Dylan J. Nagle (2), George Jung (1), Alan R. Wilson (2), Chandarin Ung (3), Wing K. Chiu (3), Greg Crew (3)

(1) Aerospace Division, Defence Science and Technology Organisation, Fishermans Bend, Victoria, Australia
(2) Maritime Division, Defence Science and Technology Organisation, Fishermans Bend, Victoria, Australia
(3) Department of Mechanical and Aerospace Engineering, Monash University, Clayton, Victoria, Australia

ABSTRACT

A vibration energy harvesting approach has been developed to harvest energy from low frequency mechanical vibrations (i.e. < 20 Hz). The energy harvester reported consists of an oscillator created using a spherical permanent-magnet, wear-pad and wire coil arrangement. A magnetic restoring force acts on the spherical magnet, and as the magnet oscillates it steers magnetic field through the transducer thereby producing an oscillating charge that can be harvested. Measured stochastic-like vibrations from three different vehicle types (i.e. jet plane, train, and boat) were reproduced on a vibration shaker. The non-optimised energy harvester's response to the three vibration spectra was examined. The largest output was in response to the train vibrations which produced a peak power of 18.5 mW and a longer term RMS power of 1.28 mW.

1. INTRODUCTION

The Australian Defence Science and Technology Organisation (DSTO) is developing a variety of in-situ structural health monitoring (SHM) approaches for potential use on high value platforms (Galea et al., 2001). The implementation of SHM systems would allow a fleet operator to reduce through-life support costs and increasing availability (Galea et al., 2009) by replacing interval based inspection and maintenance with more cost-effective condition-based approaches.

Ideally an SHM device should operate independently from the vehicle it is monitoring (Galea et al., 2009), hence a critical issue is powering of the device (Moss et al., 2010a). As an alternative to batteries, which need to be replaced or recharged (creating a maintenance issue of their own), DSTO is investigating the use of vibration energy harvesting for powering sensor systems (Moss et al., 2010b). Energy harvesting is the process of capturing available free energy from the local environment (e.g structural vibrations) and converting it into an electrical form (Beeby & White, 2010). While there are commercially available energy harvesters, performance limitations such as low power density (Kim et al, 2009) and a narrow operational frequency bandwidth (Moss et al., 2011) have prevented the widespread application of these devices.

The present paper examines two nonlinear vibration energy harvesting arrangements based on a spherical-permanent-magnet, wearpad and wire-coil arrangement. The arrangements under investigation are non-linear, so can potentially operate over a wider range of frequencies than a linear harvester (Vandewater and Moss, 2013a). The accelerations experienced in a fast-jet plane, heavy rail car train and boat, and the harvesters' reponse to each of these platforms, is described.

1.1. Principles of operation

As shown schematically in Figure 1a, the harvester consists of a vertically poled neodymium-iron-boron (NdFeB) spherical magnet ('sphere') positioned on top of a pancake coil. A small NdFeB 'centre-magnet' is located at the middle of the coil (also poled vertically), which magnetically interacts with the sphere. The sphere is free to oscillate in the x - y plane (where x is normal to the page), on a wear-pad above the coil.

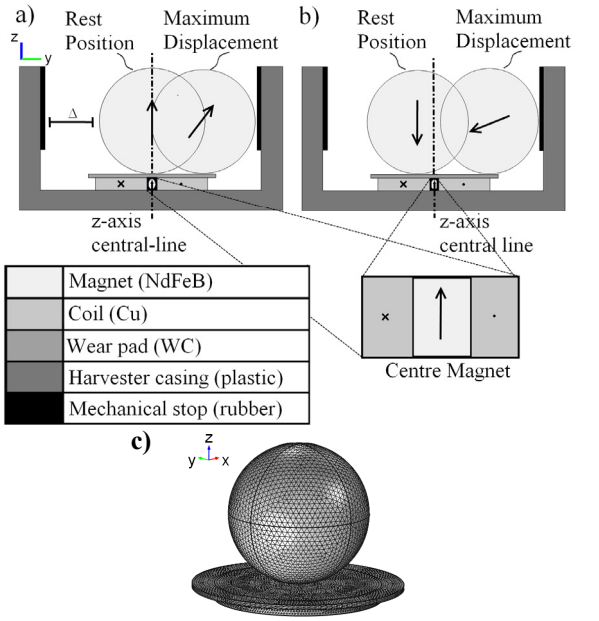

Figure 1. a) Harvester schematic showing the 'attracting fields (AF)' arrangment where the sphere is poled in the same direction as the centre-magnet at the centre of the coil. b) 'opposing fields (OF)' arrangement. c) AF harvester model showing the sphere centrally located at its rest position. Host vibration is in the x-y plane.

Due to a magnetic restoring force between the sphere and the centre magnet (and also the wear-pad) vibration of the host structure ('host vibration') will result in oscillation of the sphere. As the sphere oscillates relative to the coil, the coil experiences a changing magnetic field creating a time-varying magnetic flux through the coil. Hence, a time-varying electromotive force is induced across the coil via

Faraday's Law of Induction (Maxwell, 1904), producing current through an attached electrical load. The 'Maximum Displacement' shown in Figures 1a and 1b depicts contact between the sphere and a mechanical stop (consisting of rubber bonded to the inside of the harvester's casing). The maximum amplitude of oscillation of the sphere is determined by the gap Δ, which is the distance between the mechanical stop and the sphere's rest position (designated 'Rest Position' in Figure 1a).

This paper will explore two non-optimised harvester arrangements: (i) 'attracting fields (AF)' where the sphere and centre-magnet are poled in the same direction and (ii) 'opposing fields (OF)' where the sphere and centre magnets are poled in opposite directions.

2. EXPERIMENTAL

2.1. Host vibrations

The harvester arrangements described in section 1.1 were subjected to host vibrations from three difference vehicle types: plane (Galea et al., 2009), train (Ung et al., 2013), and boat.

Figure 2. Accelerometer locations. Upper – in-board aileron hinge of a fast jet. Centre – bogey of a heavy-haul rail-car. Lower – bow of a boat.

Figure 2 shows the accelerometer locations (on the three vehicle types) where the vibration data was recorded. The accelerations recorded from all three vehicle types were somewhat stochastic in nature. Hence, acceleration power spectral densities ('PSD'), can be calculated from the vibration data, and reproduced within the limits of a vibration shaker. PSDs' are used to produce random vibrations that follow a specified frequency-acceleration curve (Millers and Childers, 2012).

2.2. Prototype Energy Harvester

The prototype harvester schematically shown in Figure 1 was investigated using the experimental arrangement illustrated in Figure 3. The magnetic sphere (NdFeB, type N42 with remanent magnetisation ~1.3 T) has a diameter of 25.3 mm, while the centre-magnet has a 3 mm diameter and is 2 mm high. A 38 mm diameter tungsten carbide (6% cobalt by mass, grade KT20) wear-pad with thickness 0.8 mm was used to protect the upper surface of the wound coil and to provide a smooth-surface for the sphere to move on. The coil was custom wound from 71 μm diameter copper wire with approximately 3300 turns and had a height of 2 mm, an outer diameter of 26.8 mm and an inner diameter of 3 mm. Its measured inductance and resistance were 92 mH and 680 Ω respectively. As shown in Figure 3 the sphere's displacement was restricted by the harvester's circular casing, which has an internal diameter of 66.5 mm and is manufactured from plastic, using a printing process. The casing has a 6 mm wall thickness and its inside face is covered by rubber 1.7 mm thick. For both the AF and OF arrangements the average gap (Δ) is 18.9 mm. At times while being stochastically excited, the sphere would collide with the rubber coated casing and a brief period of vibro-impacting motion would ensue (Vandewater and Moss, 2013a). Note that for the OF arrangment, due to the repulsive force between the sphere and the centre-magnet the sphere's rest position is approximately 3.5 mm from the centre of the coil (see Figure 3).

2.3. Experimental Arrangement

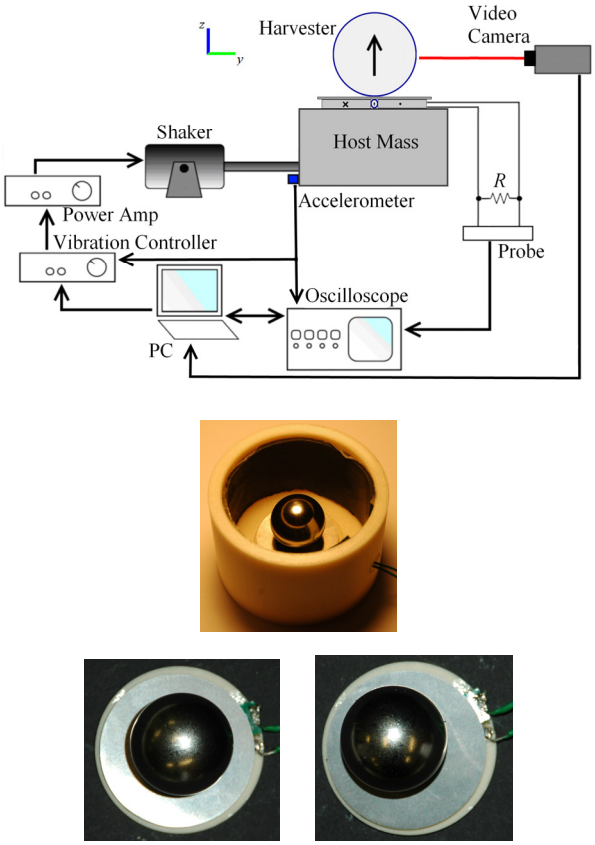

Figure 3. Upper – schematic of the experimental arrangement for measuring coil output across a matched resistive load *R* (harvester casing not shown). Middle – photo of the prototype harvesting arrangement. Lower left – sphere at rest position in 'attracting fields (AF)' harvester arrangement. Lower right – sphere at rest position in 'opposing fields (OF)' harvester arrangement, ~ 3.5 mm from centre.

As shown in Figure 3, the prototype harvester was mounted on a 'host' platform with an approximate mass of 5 kg, which was attached to a 200 N electromagnetic vibration shaker. It was necessary to apply a 2 Hz high-pass filter to the measured vehicle accelerations so that the vibration shaker was not over driven. PSD's of the three measured vibrations (plane, train and boat) were calculated and then programmed into a vibration controller (Brüel & Kjær 7541, 'controller') for reproduction. The minimum frequency bandwidth required by the PSD controller was 500 Hz wide (for bandwidths smaller than 500 Hz a chaotic shaker response was observed), so PSD's were widened to 500 Hz (at -1.5 dB/octave). It is noted that the shaker and host platform had a self-resonance near 5 Hz, however the closed loop vibration controller was able to minimise this effect when reproducing a PSD. As shown in Figure 3, a resistive load was applied and measurements of the harvesters' output voltage were made using an oscilloscope. The load resistance is 680 Ω, which corresponds to a near optimum value. RMS output power was calculated from at least 120 seconds of measured data.

3. RESULTS AND DISCUSSION

The following section will discuss the resonant frequency of the prototype harvester and the response of the harvesters to the reproduced vehicle vibrations using the shaker/host platform described in section 2.3. The output power from the prototype harvester arrangements described in section 2.2 (AF and OF, subjected to the aforementioned vibration) is also discussed. Finally, because the applied excitations are stochastic in nature, the harvester output power is compared using occurance plots.

3.1. Natural Frequency of the Prototype Harvester

3.1.1. Attracting Fields (AF)

To predict the resonant frequency of the prototype AF harvester the restoring force acting on the sphere was modelled using the software COMSOL. As the magnetic sphere moves away from the centre of the wear-pad, and centre magnet, the restoring force F_y behaves like a softening spring (Moss et al., 2012) of the form,

$$F_y = \sum_{k=0}^{7} k_i y^i \quad \textbf{(1)}$$

where y is the absolute sphere displacement (m), F_y is the magnetic force acting on the sphere in the y direction, and the polynomial coefficents k_i are effective spring constants.

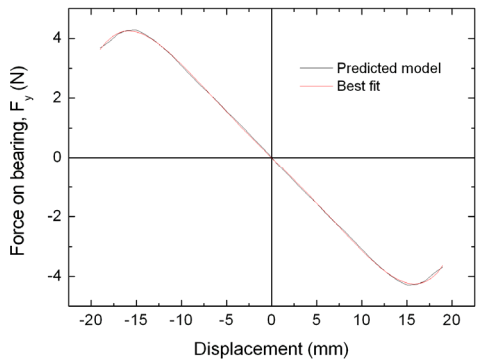

Figure 4. Predicted force on the sphere (AF design).

The spring constants were estimated from the model predictions, which were static solutions of the magnetic forces acting on the sphere as its position was stepped from one side of the wear-pad to the other. The assumed relative permeability of the WC wear-pad was $\mu_r = 10$ (Vandewater et al., 2013b). The predicted values and fitted curve are shown in Figure 4, with a maximum restoring force of 4.29 N.

The spring constants, shown in Table 1, indicate that the magnetic sphere of 64.34 g will have a natural frequency of 10.8 Hz for displacements less than 12 mm (i.e. within the linear region of the curve shown in Figure 4).

Table 1. Polynomial coefficients for Equation 1 (95% conf.)

	k0 (N)	k1 (N/m)	k2 (N/m^2)	k3 (N/m^3)	k4 (N/m^4)	k5 (N/m^5)	k6 (N/m^6)	k7 (N/m^7)
AF	0	303.3	0	2.5E5	0	-1.7E9	0	0
OF	0.19	160.1	6.6E3	1.4E6	-4.7E7	-5.0E9	6.2E10	3.9E12

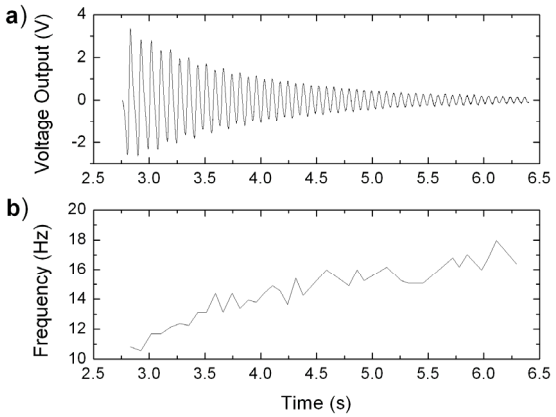

Figure 5. a) Experimental ring down and **b)** corresponding electrical frequency of the sphere (AF design). Mechanical frequency (not shown) is half of the electrical frequency.

An experimental ring down, involving manual displacement of the sphere to the edge of the wear-pad before being released, was used to experimentally confirm the natural resonance. The ring downs were performed under an electrical load of 680 Ω, with the output voltage of the harvester shown in Figure 5a. Figure 5b illustrates the frequency of the spheres' movement, calculated from the electrical output of the harvester. It is important to note that a single mechanical cycle is represented by two electrical cycles (i.e. as the sphere travels half a cycle it passes across the two sides of the coil). The mechanical frequency of the sphere will therefore be half of that shown by the electrical output. The mechanical frequency of the sphere at the start of the ring down (2.75 – 3.5 s) is shown to be quite low, ~ 5.5 - 7 Hz. This is due to the softening described in Equation 1, as the sphere is undergoing displacements greater than 12 mm. As the displacement decreases, the mechanical frequency is shown to increase to ~ 8 - 9 Hz, which is less than the predicted mechanical frequency of 10.8 Hz. It is noted that the sphere favours a slightly elliptical motion, which may explain the reduction in natural frequency when compared to the model prediction.

3.1.2. Opposing Fields (OF)

By orienting the magnetic sphere to oppose the centre-magnet a new force curve may be obtained. The WC wear-pad remains magnetized in the same direction as the sphere,

due to the ferromagnetic properties of the cobalt binder in the WC. This causes the sphere to remain attracted to the wear-pad, with a small region of opposing magnetic field from the centre-magnet in the middle of the wear-pad. As a result the sphere sits slightly off centre (~3.5 mm, as shown in Figure 3), in a much less stable position to the AF arrangement discussed in 3.1.1. The OF arrangement produces the Force-displacement curve in Figure 6, which is adequately modelled using Equation (1) with the second set of coefficients in Table 1.

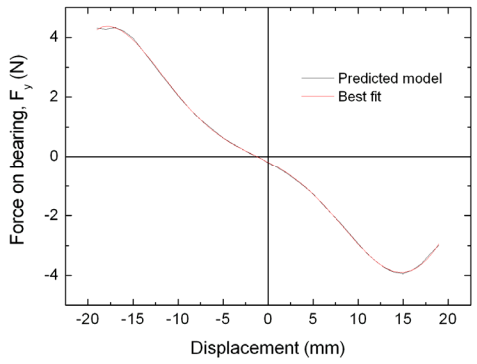

Figure 6. Predicted force on the sphere (OF design).

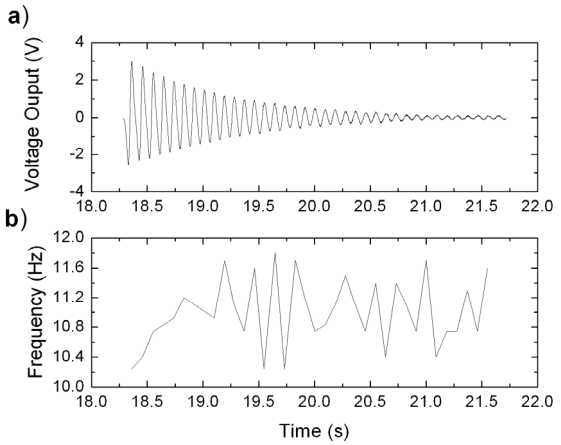

Figure 7. a) Measured experimental ring down and **b)** corresponding electrical frequency of the sphere (OF design). Mechanical frequency (not shown) is half of the electrical frequency.

Note that Figure 6 shows a minimum in F_y near $y \sim -1$ mm which is a smaller displacement than the observed stable position ~3.5 mm away from the middle of the coil (and as shown in Figure 3). The natural frequency is predicted to be at 7.9 Hz for small displacements (-5 mm $< y < 2$ mm). It was found experimentally that the sphere preferentially moves in an elliptical motion, causing the natural frequency found experimentally to be considerably lower than the model prediction. The ring down shown in Figure 7a demonstrates the magnetic sphere moving linearly for the first second (18 – 19 s) before moving into chaotic elliptical motion, illustrated by the uneven peaks after 19 s. The mechanical frequency of ~ 5 – 5.6 Hz (Figure 7b, 18 – 19 s), lower than the predicted 7.9 Hz, can be explained by the softening of the curve for large displacements (i.e. the sphere is released from $y = -19$ mm and moves into the region -5 mm $< y < 2$ mm). As the displacement becomes smaller it is expected that the mechanical frequency will increase to the predicted 7.9 Hz (14.8 Hz in the electrical output). Instead the frequency remains at a low level, with regions where the frequency rapidly increases or decreases. This can be explained by the sphere following elliptical paths of varying lengths. The exact nature of this motion will be investigated at a later date, as the focus of this paper is on the response of the two harvester designs to vibrations experienced on the plane, train and boat platforms.

3.2. Comparison of Host Vibrations

3.2.1. Jet Plane

The vibration data collected from the inboard aileron hinge of a jet plane is shown in Figure 8 (Galea et al., 2009). The PSD data shown was averaged over a number of flights with differing flight profiles (i.e. varying airspeeds and altitudes). The accelerations were recorded at 483 samples per second over a number of hours. This data was used to generate a PSD with a bandwidth of 0 to 60 Hz (which was widened to 500 Hz at -1.5 dB/octave as previously described). Structural resonances were found at 14, 30 and 55 Hz.

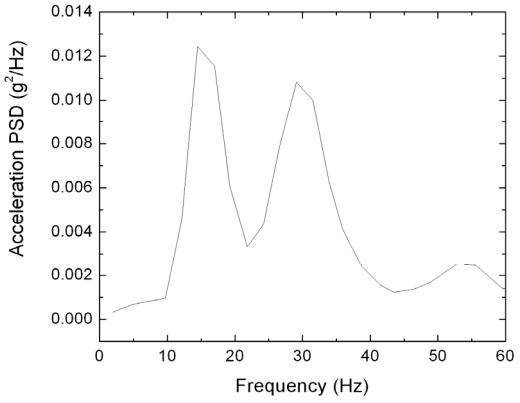

Figure 8. Typical acceleration frequency spectrum from a fast jet.

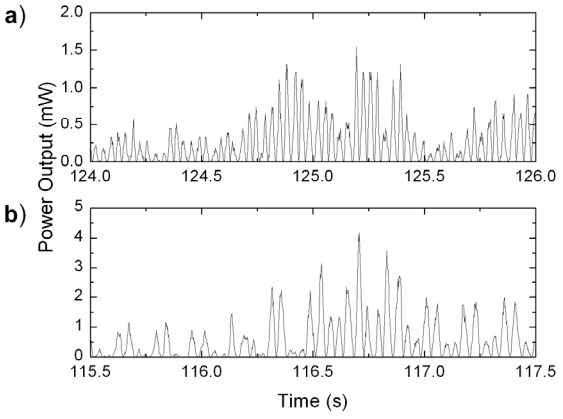

Figure 9. Measured peak power output of the **a)** AF and **b)** OF harvester designs in response to the applied fast jet accelerations.

The acceleration PSD's collected from the fast jet were the highest across the three platforms, with peaks reaching 0.012 and 0.01 g^2/Hz. The RMS acceleration was measured at 0.746 g (where 1 g = 9.8 m/s^2). These accelerations were applied to both the AF and OF designs. The recorded voltage from the prototype energy harvester measured across a matched 680 Ω resistor was used to establish the power gen-

erated. A 2 s sample of the power output, demonstrating the peak power generated for the AF and OF harvesters, is shown in Figure 9a and b respectively.

The AF harvester produced a peak power of 1.54 mW, with a RMS power of 0.1 mW. Comparatively, the OF harvester performed much better, reaching a peak of 4.18 mW and a RMS power of 0.25 mW. The AF design produced power at a higher frequency than the OF harvester, with the sphere moving at a higher velocity. The high power results for the OF design are likely due to the significant flux change as the magnetic sphere moves across the area in the centre of the coil. The central region of the coil is initially subjected to negative flux (from the centre-magnet), to positive flux as the magnetic sphere is forced across the wear-pad, resulting in a large potential difference in the coil.

3.2.2. Train

The input PSD data, collected from the heavy rail car with a sampling rate of 100 samples per second (Ung et al. 2013), is shown in Figure 10. A randomly chosen 10 minute data sample (from hours of recorded acceleration data) was used to create the PSD which has a bandwidth of 0 to 50 Hz (widened to 500 Hz at -1.5 dB/octave as previously described). Large vibration responses were found to occur in the train at 20 Hz, with smaller peaks at 10, 15, 27 and 37 Hz. These vibration responses had a peak of 0.007 g^2/Hz, with a range of smaller peaks across the frequency range of 5 to 45 Hz. The maximum peak acceleration was slightly below those occurring on the plane platform. The RMS acceleration was measured at 0.454 g, using the controller software.

The power output for both harvester designs is shown in Figure 11. As seen in the response to the aircraft accelerations, the OF design (Figure 11b) was seen to have a greater efficiency in harvesting the vibrational energy than the AF design. The peak power in the OF design reached 18.5 mW, with an RMS power of 1.28 mW, while the AF design had a peak power of 2.95 mW and RMS power of 0.24 mW. The frequency of the power produced in the OF design is again lower than that of the AF design. The OF power output does not show strictly sinusoidal movement, which is seen in the AF power output. This may be due to the vibro-impact mechanics of the sphere as it hits the walls of the harvester, distorting the natural response, a mechanism described in Vanderwater and Moss, 2013a.

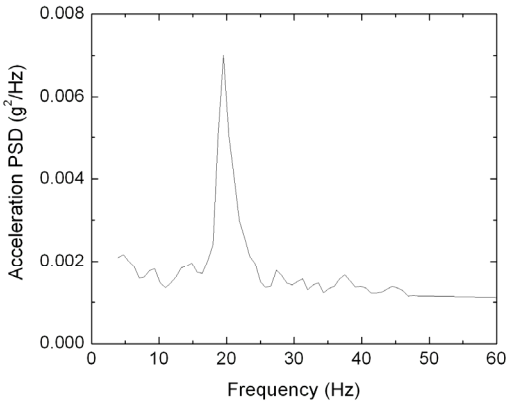

Figure 10. Typical acceleration frequency spectrum from a train.

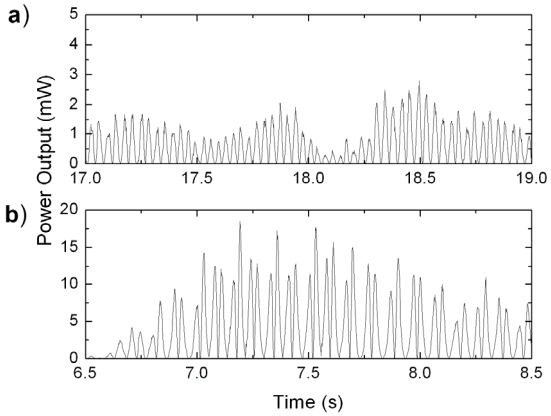

Figure 11. Peak power output of the **a)** AF and **b)** OF harvester designs in response to the applied train accelerations.

3.2.3. Boat

The acceleration data collected from near the bow of a boat (rough seas) was sampled at 50 samples per second, over a number of hours. As such the Nyquist limit was much lower than that of the other platforms (plane and train). Hence, the peak at 22 Hz, shown in Figure 12, may be a conservative estimate. A randomly chosen 10 minute data sample was used to create the PSD is from 0 to 25 Hz (widened to 500 Hz at -1.5 dB/octave as previously described). This PSD demonstrates peak accelerations at 16, 19 and 22 Hz, with minor peaks at 6 and 8 Hz. These peak accelerations had a maximum of 0.00185 g^2/Hz, considerably lower than the plane and train platforms. The target RMS acceleration was also considerably lower, at 0.275 g. This may be due to the large low frequency swells experienced by the boat being removed from the data by the applied 2 Hz filtering, and higher-frequency slamming events being undersampled by the low sampling rate, leaving only the small vibrations (perhaps from the motor, or low frequency structural bending modes).

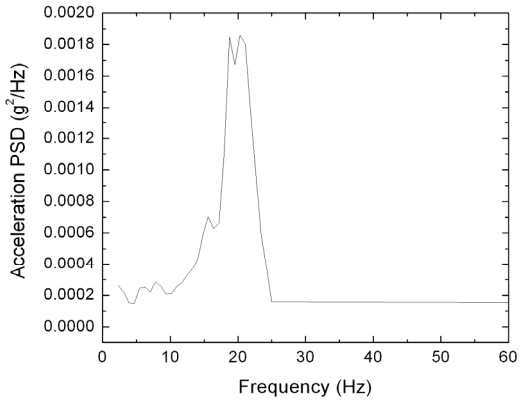

Figure 12. Typical acceleration frequency spectrum from a boat.

As seen in Figures 13a and 13b, the peak power output from the AF and OF harvester arrangements reached 0.11 mW and 1.31 mW respectively. The RMS power for the OF design was found to be 0.11 mW, with the AF design RMS power a factor of 10 lower, at 0.01 mW. Both harvester designs were observed to respond to short bursts of acceleration supplied by the boat PSD, providing a short time window of peak

power followed by much longer quiescent periods of limited energy harvesting.

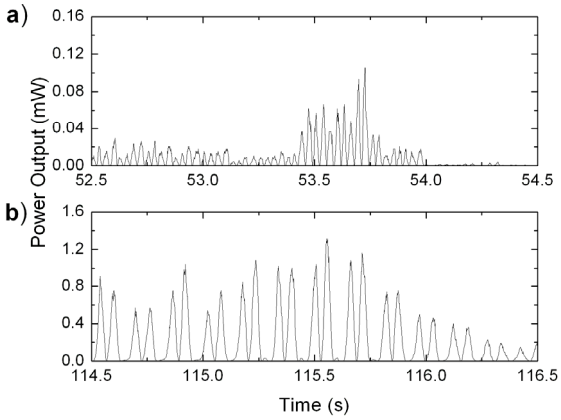

Figure 13. Peak power output of the **a)** AF and **b)** OF harvester designs in response to the applied boat accelerations.

3.3. Comparison of Harvester Output Power

The power output from each platform, for both harvester designs, is outlined in Table 2. Across both designs the train accelerations yielded the highest power output and RMS power. While the train PSD did not have the highest peak accelerations, it displayed the highest accelerations below 11 Hz (0.002 g^2/Hz). As both harvester designs were shown to have a natural frequency below 11 Hz, it is likely that these low frequency accelerations had a significant impact on the output power produced. The highest peak accelerations were seen in the plane data, which yielded the second highest power output and RMS power. These peak accelerations, at 14 and 30 Hz, may have been less effective in producing a response in the harvester as they were above the natural frequencies of the device. The accelerations at frequencies below 11 Hz were around 0.001 g^2/Hz, half of that seen in the train data. This may explain why the output power generated by the train accelerations was at least double that seen in response to the plane accelerations. The boat acceleration data averages at 0.0002 g^2/Hz for frequencies below 11 Hz, much lower than the plane and train platforms. The corresponding output power from both harvesters is the lowest of the three platforms.

Table 2. Comparison of harvester output power.

Source	Ave. Power (mW)	RMS Power (mW)	Peak Power (mW)
Attracting Fields(AF)			
Jet Plane	0.034	0.10	1.54
Train	0.10	0.24	2.95
Boat	0.002	0.01	0.11
Opposing Fields (OF)			
Jet Plane	0.11	0.25	4.18
Train	0.65	1.28	18.5
Boat	0.05	0.11	1.31

When comparing the two harvester designs, the OF harvester consistently produced a higher peak power output and RMS power than the AF harvester. The frequency plots (NIST/SEMATECH, 2012) shown in Figures 14 and 15 indicate that the instances of high power output are greatly increased in the OF design. As mentioned previously, this is likely due to the large change in flux experienced by the coil as it is subjected to the negative flux of the centre-magnet and the dominating positive flux of the bearing as it moves across the surface of the coil. The higher power output may also be explained by the friction between the sphere and the wear-pad of the AF design being higher than that of the OF design. In the AF design the sphere experiences a large force in the z direction, strengthened by the attraction of the sphere to the centre-magnet. In the OF design, the centre-magnet repels the sphere, decreasing the force and hence the amount of friction between the sphere and the wear-pad. The displacement of the sphere in the OF harvester is not inhibited by the larger frictional forces found in the AF design, allowing the sphere to move more easily in the OF design. The linear spring constant (k_1) was higher in the AF harvester, indicating that a higher force is required to initiate small displacements than in the OF design.

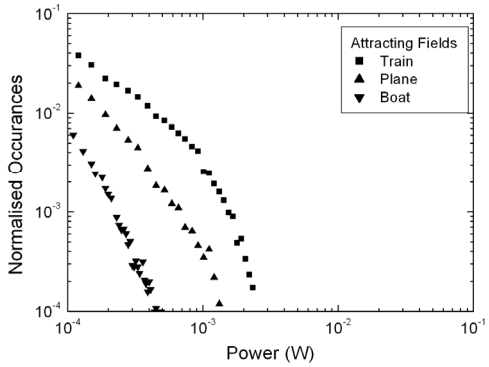

Figure 14. Distribution of power output from the AF harvester design.

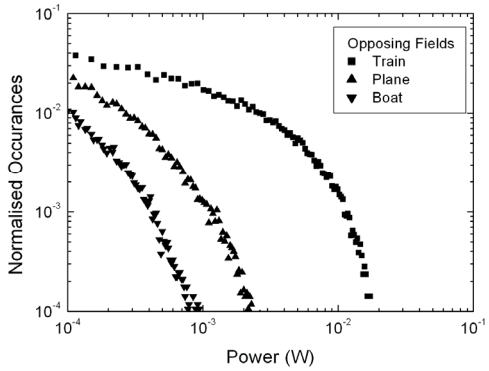

Figure 15. Distribution of power output from the OF harvester design.

As indicated in Table 2 and Figure 15, the OF device produces a useful level of electrical power from a variety of stochastic vibration sources. It is important to note that high impact (e.g. slamming) events cannot be accurately reproduced using the experimental arrangement shown in Figure 3, nor can low frequency large amplitude displacement excursions. Due to these experimental limitations, the authors believe that the given output power levels are conservative. Future experimental work will involve mounting the harvesting devices onto the actual vehicle platforms, hence exposing them to true operational vehicular vibrations.

CONCLUSION

Two prototype non-optimised harvester designs, designated as 'attracting fields (AF)' and 'opposing fields (OF)', were tested using vibration data collected from jet plane, train and boat platforms. The OF design maintained a higher measured power output across the three platforms when compared to the AF design. The highest measured power outputs of 18.5 mW peak and 1.28 mW RMS was obtained using the OF design when excited by the equivalent accelerations to the train platform, with a peak of 0.007 g^2/Hz and an RMS acceleration of 0.45 g. The accelerations in the jet plane vibration spectrum were the highest across the three platforms with a peak of 0.012 g^2/Hz and an RMS acceleration of 0.75 g, from which the OF design produced output powers of 4.18 mW peak and 0.25 mW RMS. The boat acceleration data was the lowest of the three platforms, with a peak of 0.0018 g^2/Hz and RMS acceleration of 0.28 g, from which the OF design produced 1.31 mW peak and 0.11 mW RMS. The measured output powers from the OF design indicate that the arrangement can harvest useful electrical energy from a variety of stochastic vibration sources. The authors believe that the measured output powers are conservative because the experimental arrangment used was unable to reproduce high energy impact events. A future work program was proposed involving the mounting of harvesting devices onto actual vehicle platforms.

ACKNOWLEDGEMENTS

SDM would like to acknowledge the support of the DSTO Fellowship program. GAH would like to acknowledge the support of the DSTO IEP Program, and thank Charlie Benson and Kristyn Hart for their useful discussions.The authors would like to thank David Conser and Carl Mouser for assistance with aircraft acceleration PSD data.

REFERENCES

Beeby, S & White N 2010 *Energy Harvesting for Autonomous Systems*, Artech House, Boston.

Galea S C, Powlesland I, Moss S, Konak M, van der Velden S, Stade B, and Baker A 2001, 'Development of Structural Health Monitoring Systems for Composite Bonded Repairs,' *Proceedings of SPIE*, Vol. 4327, pp. 246-257.

Galea S C, van der Velden S, Moss S, and Powlesland I 2009 *Encyclopaedia of Structural Health Monitoring: On the way to autonomy: the wireless-interrogated and self-powered 'smart patch' system*, John Wiley & Sons.

Kim H, Lee W, Rasika Dias HV, and Priya S 2009, 'Piezoelectric Microgenerators – Current Status and Challenges,' *IEEE Trans. Ultra. Ferro. Freq. Cont.*, vol. 56, p. 1555.

Maxwell J C 1904 *A treatise on electricity and magnetism vol. II* , Clarendon Press, Oxford.

Millers S and Childers D 2012. *Probability and random processes*. Academic Press.

Moss S, Powlesland I, Galea S, Carman G 2010a, 'Vibro-impacting power harvester,' *Proceedings of SPIE*, vol. 7643 (PART 1), art. no. 76431A.

Moss S, Barry B, Powlesland I, Galea S, and Carman G P 2010b, 'A low profile vibro-impacting power harvester with symmetrical stops,' *Applied Physics Letters*, vol. 97, Art. 234101.

Moss S, Barry A, Powlesland I, Galea S, and Carman GP 2011, 'A broad-band Vibro-impacting Power Harvester with Symmetrical Piezoelectric Bimorph-stops,' *Smart Materials and Structures*, vol. 20, p. 045013.

Moss S D, McLeod J E, Powlesland I J and Galea S C 2012, 'A bi-axial magnetoelectric vibration energy harvester,' *Sensors and Actuators A: Physical*, vol.175, pp. 165–168.

Moss S D, McLeod J E, Galea SC 2013, 'Wideband vibro-impacting vibration energy harvesting using magneto-electric transduction,' *Journal of Intelligent material Systems and Structures*, vol. 24, no. 11, pp. 1313-1323.

NIST/SEMATECH 2012 *e-Handbook of Statistical Methods*, http://www.itl.nist.gov/div898/handbook/ .

Vandewater LA and Moss SD 2013a, 'Probability-of-existence of vibro-impact regimes in a nonlinear vibration energy harvester,' *Smart Materials and Structures*, in press.

Vandewater LA, Moss SD, and Galea SC 2013b, 'Optimal coil transducer geometry of an electromagnetic nonlinear vibration energy harvester,' *Key Engineering Materials*, vol. 558, pp. 477-488.

Ung C, Moss SD, Vandewater LA, Galea SC, Chiu WK, Crew G 2013, 'Energy Harvesting from Heavy Haul Railcar Vibration,' *Proceedings of the IEEE International Conference on Intelligent Sensors, Sensor Networks and Information Processing*, Melbourne, Australia.